Local discrete velocity grids for deterministic rarefied flow simulations

Stéphane Brull, Luc Mieussens

Local discrete velocity grids for deterministic rarefied flow simulations

S. Brull[1], L. Mieussens[2]

[1]Univ. Bordeaux, IMB, UMR 5251, F-33400 Talence, France.
CNRS, IMB, UMR 5251, F-33400 Talence, France.
(Stephane.Brull@math.u-bordeaux1.fr)

[2]Univ. Bordeaux, IMB, UMR 5251, F-33400 Talence, France.
CNRS, IMB, UMR 5251, F-33400 Talence, France.
INRIA, F-33400 Talence, France.
(Luc.Mieussens@math.u-bordeaux1.fr)

Abstract

Most of numerical methods for deterministic simulations of rarefied gas flows use the discrete velocity (or discrete ordinate) approximation. In this approach, the kinetic equation is approximated with a global velocity grid. The grid must be large and fine enough to capture all the distribution functions, which is very expensive for high speed flows (like in hypersonic aerodynamics). In this article, we propose to use instead different velocity grids that are local in time and space: these grids dynamically adapt to the width of the distribution functions. The advantages and drawbacks of the method are illustrated in several 1D test cases.

Keywords: kinetic equations, discrete velocity model, deterministic method, rarefied gas dynamics

1 Introduction

Most of deterministic numerical methods for rarefied flow simulations are based on a discrete velocity approximation of the Boltzmann equation, see for instance [20, 18, 6, 5, 4, 15, 16, 13, 21, 11].

In almost all these methods, the distribution function is approximated with a global velocity grid, for every point in the position space, for every time. This makes the method robust (conservation, entropy dissipation, positivity, stability, etc.) and relatively simple, but very expensive for many cases. Indeed, the grid must be large enough to contain all the distribution functions of the flow, and fine enough to capture every narrow distributions. The first constraint makes the grid very large for high speed flow with large temperatures. The second constraint makes the grid step very small, and hence a very large number of discrete velocities. This is for instance the case for atmospheric re-entry problems, where the flow is hypersonic. Such cases, especially in 3D, are very difficult to be simulated with

such methods, due to the a discrete velocity grid that contains a prohibitively large number of points.

Of course, particle solvers like the popular DSMC method do not suffer of such problems [3]. However, if one is interested in deterministic Eulerian simulations, it is important to find a way to avoid the use of a too large number of discrete velocities. Up to our knowledge, there are a few papers on this subject. Aristov proposed in [1] an adaptive velocity grid for the 1D shock structure calculation. However, the approach is very specific to this test case and has never been extended. More recently, Filbet and Rey [9] proposed to use a rescaling of the velocity variable to make the support of the distribution independent of the temperature and of the macroscopic velocity. Then the Boltzmann equation is transformed into a different form (with inertia terms due to the change of referential). In [2], Baranger et al. proposed an algorithm to locally refine the velocity grid wherever it is necessary and to coarsen it elsewhere. But this approach, which has been proved to be very efficient for steady flows, is still based on a global grid, and cannot be efficient enough for unsteady flows. Finally, Chen et al. [7] proposed to use a different velocity grid for each point in the position space and every time: from one point to another one, the grid is refined or coarsen by using an AMR technique. This seems to be very efficient, but all the grids have the same bounds (they all use the same background grid). It seems that a similar method was proposed at the same time by Kolobov et al., see [14, 12].

In this paper, we propose a method that has several common features with the method of [22] and [9] but is still very different. The main difference is that each distribution is discretized on its one velocity grid: each grid has its own bounds and step that are evolved in time by using the conservation laws. The interaction between two space cells requires to use reconstruction techniques to approximate a distribution on different velocity grids. This paper is a preliminar work, for 1D flows, that proposes a complete algorithmic approach. Several test cases illustrate the properties of the method and show its efficiency.

The outline of the paper is the following. In section 2 is presented a simple 1D kinetic BGK model and its standard discrete velocity approximation. In section 3, the local discrete velocity grid approach is described. The numerical tests are given in section 4.

2 A simple 1D kinetic model and its standard velocity discretization

We consider a one-dimensional gas described by the mass density of particles $f(t,x,v)$ that at time t have the position x and the velocity v. The corresponding macroscopic quantities can be obtained by the moment vector $U(t,x) = \langle mf(t,x,.)\rangle$, where $m(v) = (1, v, \frac{1}{2}|v|^2)$ and $\langle\phi\rangle = \int_{\mathbb{R}} \phi(v)\, dv$ for any velocity dependent function. This vector can be written component wise by $U = (\rho, \rho u, E)$, where ρ, ρu, and E are the mass, momentum, and energy densities. The temperature T of the gas is defined by relation $E = \frac{1}{2}\rho|u|^2 + \frac{1}{2}\rho RT$, where R is the gas constant.

The evolution of the gas is governed by the following BGK equation

$$\partial_t f + v\partial_x f = \frac{1}{\tau}(M(U) - f), \tag{1}$$

where $M(U)$ is the local Maxwellian distribution defined through the macroscopic quantities U of f by

$$M(U) = \frac{\rho}{\sqrt{2\pi RT}} \exp\Big(-\frac{|v-u|^2}{2RT}\Big), \tag{2}$$

and $\tau = CT^\omega/\rho$ is the relaxation time. The constant C and ω will be given in section 4 for each test case.

From this equation, it is easy to establish the so called conservation laws that describe the time evolution of the moment vector U:

$$\partial_t U + \partial_x \langle mf \rangle = 0. \tag{3}$$

For the numerical approximation of equation (1), a popular method is the discrete ordinate–or discrete velocity–method. It consists in choosing a grid $\mathcal{V}$ of K points v_k, and then in replacing the kinetic equation (1) by the finite set of K equations

$$\partial_t f_k + v_k \partial_x f_k = \frac{1}{\tau}(M_k(U) - f_k) \tag{4}$$

where $f_k(t,x)$ is an approximation of $f(t,x,v_k)$ and $M_k(U)$ is an approximation of $M(U)(v_k)$.

In order to describe the solution correctly, the discrete velocity grid $\mathcal{V}$ must capture all the distribution functions, that is to say at any time t, and for every position x. This means that $\mathcal{V}$ must be large enough to capture distributions with large mean velocity or large temperature, and fine enough to capture distributions with small temperature. See an illustration of this problem in figure 1. In this figure, we show a 2D aerodynamical flow with three typical distributions functions (one in the upstream flow, one in the shock, and another one at the boundary). The corresponding velocity grid is shown in the same figure.

Such a grid can be constructed as follows. We assume that a given distribution function whose corresponding mean velocity and temperature u and T can be well described if we restrict to the interval $[u-4\sqrt{RT}, u+4\sqrt{RT}]$. This choice is reasonable, since in most physical problems, distributions are quite localized and they are concentrated in an interval which is not too far from the support of their local Maxwellian. Consequently, a first constraint, which necessary for all the distributions can be captured by the global velocity grid, is that its bounds v_{min} and v_{max} satisfy the following inequalities:

$$v_{min} \le \min_{t,x}\big(u(t,x) - 4\sqrt{RT(t,x)}\big), \qquad v_{max} \ge \max_{t,x}\big(u(t,x) + 4\sqrt{RT(t,x)}\big). \tag{5}$$

Since it is reasonable to require that there are at least three points between the inflexion points of any Maxwellian, the step of the global grid should be such that

$$\Delta v \le \min_{t,x} \sqrt{RT(t,x)}. \tag{6}$$

Of course, such an approach requires to first estimate some bounds on the macroscopic fields that are global in time and space. Even if it is rarely mentioned in the literature, we believe that this is more or less the way people do when they use numerical simulations by using discrete velocity approximations.

Note that the points of $\mathcal{V}$ are not necessarily uniformly reparted, since the grid could be refined only wherever it is necessary and coarsened elsewhere, as it is proposed in [8] for steady flows (with a simple and automatic way to define such a grid). However, for unsteady problems, the situation is more complex. Indeed, first, the estimations of the correct bounds and step of the grid are not necessarily available for every problems (the velocity or the temperature could reach much larger values that were not expected at some times of the simulation), like in complex shock interactions, for instance. Moreover, even if it is possible, this could lead to a grid which is extremely large and dense, hence leading to a very expensive simulation (see an example in section 4.2).

It is therefore very attractive to try to use *local* velocity discretization of the distribution function, which means to use a *local discrete velocity grid* (LDV) for each time and position. In other words, we would like to approximate $f(t, x, .)$ with one different grid for each t and x. The clear advantage of this idea is that we can defined an optimally small grid for each distribution, thus we avoid the problems mentioned above. This approach is developed in the next section.

3 A local discrete velocity grid approach

In this section, we describe the basic algorithm that allows us to use local discrete velocity grids. Then we give some details about the reconstruction step, and we suggest possible definition of non symmetric grids.

3.1 The method

Now we assume that at time t_n, the distribution function in each space cell $[x_{i-\frac{1}{2}}, x_{i+\frac{1}{2}}]$ is approximated on a set $\mathcal{V}_i^n$ of K local discrete velocities (the local discrete velocity grid, LDV for short) for $i \in \{0, i_{max}+1\}$. The cells $[x_{i-\frac{1}{2}}, x_{i+\frac{1}{2}}]$ for $i \in \{1; i_{max}\}$ represent the cells inside the domain. For simplicity, we assume here that all the local grids have the same number of points K, and the points are equally reparted. The first point is denoted by $v_{min,i}^n$ and the last one by the $v_{max,i}^n$. That is to say, we have for $i \in \{0, i_{max}+1\}$:

$$\mathcal{V}_i^n = \left\{ v_{i,k}^n = v_{min,i}^n + k\Delta v_i^n, \quad k = 1 : K \right\}, \qquad \text{where} \qquad \Delta v_i^n = \frac{v_{max,i}^n - v_{min,i}^n}{K}.$$

The velocity grids $\mathcal{V}_0^n$ and $\mathcal{V}_{imax+1}^n$ represent the velocity grids associated to the fictious cells. On this local grid, $f(t_n, x_i, .)$ is approximated by K values that are stored in the vector $f_i^n = (f_{i,k}^n)_{k=1}^K$. Each discrete value $f_{i,k}^n$ is an approximation of $f(t_n, x_i, v_{i,k}^n)$.

The corresponding macroscopic quantities $U(t_n, x_i)$ are approximated by U_i^n with the following quadrature formula

$$U_i^n = \langle m f_i^n \rangle_{\mathcal{V}_i^n} = \sum_{k=1}^{K} m(v_{i,k}^n) f_{i,k}^n \omega_k, \tag{7}$$

where the ω_k are the weights of the quadrature.

When one wants to compute an approximation of f at the next time step t_{n+1}, two problems occur. First, how to determine the local discrete velocity grid $\mathcal{V}_i^{n+1}$? We will show below that this can be simply made by using the conservation laws. Second, how to exchange information between two space cells, since the local grids are not the same? This is where we use some interpolation procedure in the method. Let us now describe our algorithm step by step.

Step 1: Macroscopic quantities at t_{n+1}.

We approximate the conservation relation (3) with the following first order upwind scheme

$$U_i^{n+1,\star} = U_i^n - \frac{\Delta t}{\Delta x}\left(\Phi_{i+\frac{1}{2}}^n - \Phi_{i-\frac{1}{2}}^n\right), \tag{8}$$

where the numerical fluxes are defined by

$$\Phi_{i+\frac{1}{2}}^n = \left\langle v^+ m f_i^n \right\rangle_{\mathcal{V}_i^n} + \left\langle v^- m f_{i+1}^n \right\rangle_{\mathcal{V}_{i+1}^n}, \tag{9}$$

which is indeed an approximation of the flux $\left\langle vmf(t_n, x_{i+\frac{1}{2}}) \right\rangle$ at the cell interface. Here, we use the standard notation $v^\pm = (v \pm |v|)/2$. Note that each half flux is computed on the local velocity grid of the corresponding distribution. The vector $U_i^{n+1,\star}$ is an approximation of $U(t_{n+1}, x_i)$, and we note $u_i^{n+1,\star}$ and $T_i^{n+1,\star}$ the corresponding velocity and temperature.

Step 2: discrete velocity grid $\mathcal{V}_i^{n+1}$.

We define this grid by using the new velocity and temperature $u_i^{n+1,\star}$ and $T_i^{n+1,\star}$ to get the bounds

$$v_{min,i}^{n+1} = u_i^{n+1,\star} - 4\sqrt{RT_i^{n+1,\star}} \quad \text{and} \quad v_{max,i}^{n+1} = u_i^{n+1,\star} + 4\sqrt{RT_i^{n+1,\star}}. \tag{10}$$

Then the new grid $\mathcal{V}_i^{n+1}$ is defined as in the previous time step, that is to say by

$$\mathcal{V}_i^{n+1} = \{v_{i,k}^{n+1} = v_{min,i}^{n+1} + k\Delta v_i^{n+1}, \quad k = 1 : K\}, \text{with} \quad \Delta v_i^{n+1} = (v_{max,i}^{n+1} - v_{min,i}^{n+1})/K.$$

Step 3: distribution function at time t_{n+1}.

Here, equation (1) is approximated by a first order upwind scheme, with an implicit relaxation term. If the velocity variable is not discretized, we get for every v:

$$\begin{aligned} f_i^{n+1}(v) = f_i^n(v) - \frac{\Delta t}{\Delta x} v^+ (f_i^n(v) - f_{i-1}^n(v)) - \frac{\Delta t}{\Delta x} v^- (f_{i+1}^n(v) - f_i^n(v)) \\ + \frac{\Delta t}{\tau_i^{n+1}} (M(U_i^{n+1,\star})(v) - f_i^{n+1}(v)). \end{aligned}$$

If now we take into account that each distribution f_i^{n+1}, f_i^n, f_{i-1}^n, and f_{i+1}^n are defined on their own local velocity grid, this scheme must be modified by using a reconstruction procedure. Then we define the discrete values of f_i^{n+1} on its grid $\mathcal{V}_i^{n+1}$ by

$$f_{i,k}^{n+1} = \bar{f}_i^n(v_{i,k}^{n+1}) - \frac{\Delta t}{\Delta x} v_{i,k}^{n+1^+}(\bar{f}_i^n(v_{i,k}^{n+1}) - \bar{f}_{i-1}^n(v_{i,k}^{n+1})) - \frac{\Delta t}{\Delta x} v_{i,k}^{n+1^-}(\bar{f}_{i+1}^n(v_{i,k}^{n+1}) - \bar{f}_i^n(v_{i,k}^{n+1})) + \frac{\Delta t}{\tau_i^{n+1}}(M_k(U_i^{n+1}) - f_{i,k}^{n+1}), \tag{11}$$

for $k = 1$ to K. In this relation, the distributions f_i^n, f_{i-1}^n, and f_{i+1}^n are used to reconstruct piecewise continuous in velocity functions $\bar{f}_i^n$, $\bar{f}_{i-1}^n$, and $\bar{f}_{i+1}^n$ that are defined as follows:

$$\bar{f}_i^n(v) = \begin{cases} p_i^n(v) & \text{if } v_{min,i}^n \leq v \leq v_{max,i}^n \\ 0 & \text{else,} \end{cases} \tag{12}$$

where p_i^n is a piecewise continuous function of v constructed through the values $(v_{i,k}^n, f_{i,k}^n)_{k=1}^K$, like a piecewise interpolated polynomial. This reconstruction will be discussed in next section.

Step 4: Corrected macroscopic quantities.

Here, we compute the moments of f_i^{n+1} by the quadrature formula (7) to get

$$U_i^{n+1} = \left\langle m f_i^{n+1} \right\rangle_{\mathcal{V}_i^{n+1}} = \sum_{k=1}^K m(v_{i,k}^{n+1}) f_{i,k}^{n+1} \omega_k. \tag{13}$$

Note that U_i^{n+1} is an approximation of $U(t_n, x_i)$, like the vector $U_i^{n+1,\star}$ computed at step 1. This new step might be avoided by setting $U_i^{n+1} = U_i^{n+1,\star}$, but it turns that it is required to ensure the positivity of our scheme, as it is stated below.

Property 3.1. *Assume that for every cell i, f_i^n is non negative at each point of its local velocity grid and that the corresponding reconstructed piecewise function $\bar{f}_i^n$ is non negative for every v. Finally, assume that $T_i^{n+1,\star}$ is positive for every i. Then under the CFL condition $\Delta t \leq \Delta x / \max_{i,k}(|v_{i,k}^{n+1}|)$, $f_{i,k}^{n+1}$ is also non negative at each point of its local velocity grid, for every space cell.*

Proof. As it is standard for the upwind scheme for convection problems, it is sufficient to note that (11) can be written as a linear combination of $\bar{f}_i^n$, $\bar{f}_{i-1}^n$, $\bar{f}_{i+1}^n$, and $M(U_i^{n+1,\star})$. The CFL condition of the proposition ensures that the coefficients of this combination are non negative, which gives the result. □

To conclude this section, we comment on the assumption on the sign of $T_i^{n+1,\star}$. Of course, this temperature must be positive, since it is used to define the local velocity grid

$\mathcal{V}_i^{n+1}$ at step 2. However, it seems hardly possible to prove that this property is true for the scheme presented above. Nevertheless, we want to show below that a simple modification of the scheme is sufficient to ensure the positivity of this temperature. Indeed, we propose to replace the quadratures used to compute the macroscopic vector U_i^n and the numerical flux $\Phi_{i+\frac{1}{2}}^n$ (see (7) and (9)) by the exact integral of the corresponding reconstructed functions, that is to say:

$$U_i^n = \left\langle m\bar{f}_i^n \right\rangle, \qquad \Phi_{i+\frac{1}{2}}^n = \left\langle v^+ m\bar{f}_i^n \right\rangle + \left\langle v^- m\bar{f}_{i+1}^n \right\rangle.$$

If the reconstruction procedure uses a polynomial interpolation, these integrals are just half integrals of piecewise polynomial functions and can be evaluated explicitly. With this definition, we rewrite the discrete conservation law (8) as

$$U_i^{n+1,\star} = \left\langle m\Big((1 - \frac{\Delta t}{\Delta x}|v|)\bar{f}_i^n + \frac{\Delta t}{\Delta x}v^+\bar{f}_{i-1}^n - \frac{\Delta t}{\Delta x}v^-\bar{f}_{i+1}^n\Big)\right\rangle = \langle m\phi\rangle$$

where ϕ is a piecewise continuous function of v. Now we have the following property.

Property 3.2. *Under the CFL condition $\Delta t \leq \Delta x / \max_{i,k}(|v_{i,k}^n|)$, the function ϕ is non negative, and hence $T_i^{n+1,\star}$ is positive.*

Proof. Observe that ϕ is a linear combination of $\bar{f}_i^n$, $\bar{f}_{i-1}^n$, $\bar{f}_{i+1}^n$. The last two coefficients are always non negative. As a consequence of the CFL condition, the first coefficient, which is $1 - \frac{\Delta t}{\Delta x}|v|$, is non negative if $|v|$ is small enough (that is to say $|v| \leq \max_{i,k}(|v_{i,k}^n|)$). If v is larger, the coefficient is negative, but by construction $f_i^n(v) = 0$. Consequently, ϕ is non negative for every v, and hence $U_i^{n+1,\star}$ is realized by a non negative distribution. It is then a standard result that the corresponding density, energy and temperature are positive. □

Remark 3.1. Note that this CFL condition for the positivity of $T_i^{n+1,\star}$ makes Δt depend on the $v_{i,k}^n$, while the CFL condition for the non-negativity of f_i^{n+1} (see property 3.1) makes Δt depend on the $v_{i,k}^{n+1}$. This means that our modified scheme requires two time steps: a first one to compute $U_i^{n+1,\star}$, and another one to compute f_i^{n+1}. These time steps might be slightly different.

However, we observe that in practice, even the original method (with quadratures and only one time step) preserves the positivity. This is why we do not use the modified scheme in the numerical tests presented in this paper.

3.2 Interpolation step

To compute $\bar{f}_i^n(v_{i,k}^{n+1})$ in equation (11), we have to use a reconstruction procedure. First, if $v_{i,k}^{n+1}$ is external to $\mathcal{V}_i^n$, we set $\bar{f}_i^n(v_{i,k}^{n+1}) = 0$. If $v_{i,k}^{n+1}$ is inside $\mathcal{V}_i^n$, it is not a node of $\mathcal{V}_i^n$ in general, and we use a piecewise polynomial interpolation. We observed that first order polynomial interpolation is not accurate enough. However, higher order interpolation

produces oscillations, especially in very rarefied regimes, which is probably due to the large velocity gradients (an even discontinuities) of the distribution functions in such regimes.

Consequently, we use the essentially non oscillatory (ENO) interpolation (see [19] or [10]): with 3 or 4 point ENO interpolation, the accuracy is good and there is almost no oscillation.

The reconstruction algorithm is summarized below.

1. If $|v_{i,k}^{n+1}| > \max(|v_{min,i}^n|, |v_{max,i}^n|)$, then set $\bar{f}_i^n(v_{i,k}^{n+1}) = 0$
2. else
   (a) find the interval $[v_{i,k'}^n, v_{i,k'+1}^n]$ inside $\mathcal{V}_i^n$ that contains $v_{i,k}^{n+1}$
   (b) compute the q point ENO polynomial function P defined on the stencil $\{v_{i,k'-(q-1)}^n, v_{i,k'+q}^n\}$
   (c) set $\bar{f}_i^n(v_{i,k}^{n+1}) = P(v_{i,k}^{n+1})$

Of course, the same procedure is applied to the other reconstructed values $\bar{f}_{i+1}^n(v_{i,k}^{n+1})$ and $\bar{f}_{i-1}^n(v_{i,k}^{n+1})$ in (11).

3.3 Non symmetric local discrete velocity grids

When the flow is far from equilibrium, the distribution function are different from their local Maxwellian, and might have a non symmetric shape. In particular, their support might be non symmetric as well (see for instance the heat transfer problem in the rarefied regime as shown in section 4.3. However, the local grids defined in section 3.1 are based on the local Maxwellian are are necessarily symmetric. In this section, we propose a method to modify the grid if necessary.

First, note that up to now, we have defined uniform local grids with a constant number of points. However, the method is readily extended to non uniform grids with a variable number of points : we just have to replace K by K_i^n ad ω_k by $\omega_{i,k}^n$ in every expressions of section 3.1.

Then, the idea is to enlarge the grid $\mathcal{V}_i^{n+1}$ if $f_{i,k}^{n+1}$ is not small enough at its boundaries. This is made as follows.

We perform a splitting between the relaxation step and the transport step. We first compute the intermediate quantity $f_{i,k}^{n+1/2}$ by using the transport equation as

$$f_{i,k}^{n+1/2} = \bar{f}_i^n(v_{i,k}^{n+1}) - \frac{\Delta t}{\Delta x} v_{i,k}^{n+1^+}(\bar{f}_i^n(v_{i,k}^{n+1}) - \bar{f}_{i-1}^n(v_{i,k}^{n+1})) - \frac{\Delta t}{\Delta x} v_{i,k}^{n+1^-}(\bar{f}_{i+1}^n(v_{i,k}^{n+1}) - \bar{f}_i^n(v_{i,k}^{n+1})), \tag{14}$$

for $k = 1$ to K. At the end of the transport step, the values of the distribution function $f_i^{n+1/2}$ at the boundary points $v_{i,max}^{n+1}$ and $v_{i,min}^{n+1}$ of $\mathcal{V}_i^{n+1}$ are compared to the maximum value of the distribution on the grid. If these boundary values are not small enough, new grid points $w_R = v_{i,max}^{n+1} + \Delta v_i^{n+1}$ and $w_L = v_{i,min}^{n+1} - \Delta v_i^{n+1}$ are added outside the grid by using again the transport step, until they are small enough. At the end of this step, the modified

grid $\mathcal{V}_i^{n+1}$ now has K_i^{n+1} velocities. Finally, $f_{i,k}^{n+1}$ is obtained from the relaxation step through the relation

$$f_{i,k}^{n+1} = f_{i,k}^{n+1/2} + \frac{\Delta t}{\tau_i^{n+1}}(M_k(U_i^{n+1}) - f_{i,k}^{n+1}), \tag{15}$$

for $k = 1$ to K_i^{n+1}.

It would also be interesting to use an automatic refinement of the local grid around the possible discontinuities, but this is not studied in this paper.

4 Numerical results

In this section we present three numerical tests to illustrate the main features of our method (denoted by LDV, for local discrete velocity grid). It is compared to a standard discrete velocity method (with a global velocity grid) denoted by DVM. First, the numerical scheme is tested on the Sod test case for three different regimes: the rarefied, fluid, and free transport regimes. The second test is the two interacting blast waves problem in which very high temperature differences make the standard DVM unefficient. The third test case is devoted to the heat transfer problem, where the use of non symmetric local grids is shown to be necessary when the Knudsen number increases. In these tests, the gas constant R is 208.1, except for the free transport regime in section 4.1.3 where $R = 1$.

4.1 Sod test case

4.1.1 Rarefied regime

We consider a classical Sod test in a rarefied regime for the BGK model (1) with the parameters $\omega = -0.19$ and $C = 1.08 \cdot 10^{-9}$ used in the relaxation time τ. The space domain is the interval $[0, 0.6]$ discretized with 300 points. The initial condition is the local Maxwellian distribution whose macroscopic quantities are given by:

$$\begin{aligned} &T(x) = 0.00480208,\ \rho(x) = 0.0001,\ u(x) = 0 \text{ for } x \in [0, 0.3] \\ &T(x) = 0.00384167,\ \rho(x) = 0.0000125,\ u(x) = 0 \text{ for } x \in]0.3, 0.6]. \end{aligned} \tag{16}$$

The DVM and LDV methods are compared to a reference solution given by the DVM method computed for a large and fine velocity grid (obtained after a convergence study). This velocity grid has 600 points uniformly reparted in the interval $[v_{min}, v_{max}]$ where

$$v_{min} = \min_{t,x}\big(u(t,x) - 6\sqrt{RT(t,x)}\big), \quad v_{max} = \max_{t,x}\big(u(t,x) + 6\sqrt{RT(t,x)}\big) \tag{17}$$

Of course, such bounds cannot be determined a priori, and several computations with larger and larger velocity grids have to be done before the correct bounds are found. This illustrates the difficulty to use a standard DVM when the extreme values of the velocity and the

temperature are not known a priori. Indeed, here, the temperature in the shock after the initial time is higher than the two initial left and right temperatures. If the velocity grid is computed with formula (5) and (6), when the bounds are estimated with the initial values of T and u, then it is not large enough, and the results are not correct, even if the number of velocities is increased so as to reach the grid convergence which is obtained here with 100 velocities. This is shown in figure 2.

At the contrary, our LDV method dynamically adapts to the time variations of u and T and gives very accurate results with 30 discrete velocities only in each local grid, as it is shown in figure 2. Consequently, the LDV method is very efficient for this case.

Note that in this test, the reconstruction procedure used the 4-points ENO interpolation, see section 4.1.3 for an analysis of the influence of the order of interpolation.

4.1.2 Fluid regime

Now, we consider the same Sod test case, but in the fluid regime. This regime corresponds to the limit case of equation (1) when τ is set to 0. Note that since both DVM and LDV methods are used with a time semi-implicit scheme, taking $\tau = 0$ means that f^{n+1} is set to $M(U^{n+1})$ at each time step, and hence we get two different numerical schemes for the compressible Euler equations of gas dynamics.

Here, the reference DVM has 100 velocities only. The DVM with the grid computed with the initial temperatures and velocity has also 100 velocities, but it still gives incorrect values (see figure 3), for the same reasons as mentioned in the previous section. At the contrary, our LDV method gives very accurate results with 10 velocities only.

Note that here, step 3 of our scheme is nothing but the projection step $f_i^{n+1} = M(u_i^{n+1,\star})$, and hence the choice of the interpolation procedure has no influence.

4.1.3 Free transport regime

We consider the free transport regime corresponding to the limit case in (1) when τ tends to $+\infty$. In this subsection, we take $R = 1$ and the standard non dimension values for the Sod test case. The space domain is $[-1, 1]$ and is discretized with 300 points. The distribution function is initialized by the local Maxwellian distribution function with

$$\begin{array}{c} \rho = 1,\ u = 0,\ p = 1,\ \text{in } [-1, 0[, \\ \rho = 0.125,\ u = 0,\ p = 0.1 \text{ in } [0, 1]. \end{array} \tag{18}$$

For this test case the numerical results are compared to an analytical solution of the free transport equation.

It is very difficult to accurately approximate the free transport equation with a standard DVM: the macroscopic profiles obtained with the DVM show several plateaux. These plateaux are not due to the space and time approximation, but are only due to the velocity discretization. Indeed, it can be easily proved that the macroscopic profiles of the DVM solution at time t have plateaux of length $t\Delta v$, where Δv is the step of the global uniform grid.

This is clearly seen in figures 4–6 (top), where the DVM has 30 discrete velocities. This phenomenon is known as the ray effect that appears with the discrete ordinate approximations of the radiative transfer equation.

When we test this problem with our LDV method, with 2 point piecewise interpolation, and 30 velocities in each local grids, the results are very bad: we observe very large oscillations (see figures 4–6, bottom). This is probably due to the fact that this interpolation is not accurate enough. Then we use 3 and 4 point ENO interpolation, and we observe in the same figures that the solution is now much closer to the exact solution. Moreover, while we have the same number of discrete velocities in each local grid as in the DVM, we observe that the plateaux are completely eliminated.

However, there are still some oscillations in the results obtained with the LDV. This is probably due to the fact that these results were obtained without the moment correction step 4 of our algorithm (see (13)). Indeed, if we do now the same simulation with this moment correction step, the results are very good: there are no oscillation at all, no plateau phenomenon, and the results are much closer to the analytical solution, see figures 7–9.

4.2 Two interacting blast waves

This section is devoted to the test case called "the two interacting blast waves" (see [17]). Here, the relaxation time is defined with $\omega = -0.19$ and $C = 1.08\,10^{-9}$. The space domain is the interval $[0, 1]$ which is still discretized with 300 points. The initial distribution function is a local Maxwellian distribution which macroscopic quantities are given by $\rho = 1$ and $u = 0$ everywhere, and

$$T = 4.8, \text{ in } [0, 0.1], \quad T = 4.8\,10^{-5} \text{ in }]0.1, 0.9], \quad T = 4.8\,10^{-1} \text{ in }]0.9, 1].$$

On the left and right boundaries, we use Neumann boundary conditions.

Here, the bounds of the global grid of the DVM are determined by the largest initial temperature, and its step size is given by the smallest initial temperature. Then we find that the coarsest global grid that satisfies conditions (5–6) has not less than 2 551 velocities! In figures 10–12, we observe that the LDV method requires only 30 velocities to give results that are very close to the DVM method (with 2551 velocities), both before and after the choc. This proves the high efficiency of the LDV approach for this case. Note that here again, we use a 4 point ENO interpolation in the LDV method.

4.3 Heat transfer problem

In this test, we consider the evolution of a gas enclosed between two walls kept at temperature $T_L = 300$ and $T_R = 1000$. At these walls, the distribution function satisfies the diffuse boundary condition

$$f(x = 0, v > 0) = M_{\rho_L, 0, T_L}, \quad f(x = 1, v < 0) = M_{\rho_R, 0, T_L} \tag{19}$$

where

$$\rho_L = -\frac{\int_{v<0} v f(x=0,v)dv}{\int_{v>0} v M_{1,0,T_L} dv}, \quad \sigma_R = -\frac{\int_{v>0} v f(x=1,v)dv}{\int_{v<0} v M_{1,0,T_R} dv}, \tag{20}$$

and $M_{\rho,0,T}$ denotes $\rho/\sqrt{2\pi RT}\exp(-v^2/2RT)$ for every ρ and T. The initial data is the Maxwellian with density ρ_0 (to be defined later), velocity $u_0 = 0$, and $T_0 = T_L = 300$. Here, the relaxation time is defined with $\omega = -0.5$ and $c = 6.15 \cdot 10^{-9}$.

The boundary conditions are taken into account in our numerical scheme by a ghost cell technique, as it is standard in finite volume schemes. Left and right ghost cells are defined for $i = 0$ and $i = i_{max} + 1$, and the velocity grids $\mathcal{V}_0^n$ and $\mathcal{V}_{i_{max}+1}^n$ in these cells are defined so as to correctly describe the corresponding wall Maxwellians. Then, the density ρ_L and ρ_R, that are defined as the ratio of an outgoing mass fluxes at a wall to the corresponding incoming Maxwellian mass flux, are approximated by using the boundary cell and the corresponding ghost cell, that is to say:

$$\rho_L = -\frac{\langle v^- f_1^n \rangle_{\mathcal{V}_1^n}}{\langle v^+ M(1,0,T_L) \rangle_{\mathcal{V}_0^n}}, \quad \rho_R = -\frac{\langle v^+ f_{i_{max}}^n \rangle_{\mathcal{V}_{i_{max}}^n}}{\langle v^- M(1,0,T_R) \rangle_{\mathcal{V}_{i_{max}+1}^n}}.$$

For this test case several Knudsen number can be used. This number is parametrized by the initial density ρ_0. We first analyze the LDV method in the transitional regime ($\rho_0 = 0.1$, which gives $Kn = 10^{-2}$): here, both the LDV and DVM are converged with 30 velocities, while the space domain $[0, 1]$ is discretized with 1000 points. However, the results obtained with the LDV are not accurate enough (see figure 13). An analysis of this problem shows that this is due to the local grid close to the right boundary which is not large enough: for small times, the distributions at these points are highly non symmetric.

To correct this problem, we use the algorithm proposed in section 3.3 to enlarge the local grids in a non symmetric way. Then, the LDV with 30 velocities now gives results that are indistinguishable from the DVM, see figure 14.

Finally, we test the LDV method in the rarefied regime ($Kn = 1$): the LDV (with enlarged non symmetric local grids) and the DVM are converged with 300 velocities, while the space domain $[0, 1]$ is discretized with 300 points. Here again, both methods give results that are almost indistinguishable (see figure 15). Unfortunately, the number of velocities required to get converged results is very large here, even for the LDV (300 velocities). This is probably due to the fact that the distribution function is discontinuous with respect to the velocity in this test, with very large jumps: our velocity grids, even the local ones, are uniform, and cannot capture these discontinuities when the number of velocities is too small. However, we show in figure 16 the results obtained with 50 velocities only, and we observe that the LDV gives results that are more accurate than the DVM.

Remark 4.1. Note that in these tests on the heat transfer problem, we use the moment correction step, otherwise, some sharp oscillations appear at some points. For large Knudsen numbers, this correction step is essential, since the oscillations can be very large.

Moreover, note the interpolation procedure has been performed with a 4 points ENO method, and no improvements are observed if we use larger stencils.

5 Conclusion and perspectives

We have presented a new velocity discretization of kinetic equations of rarefied gas dynamics: in this method, the distribution functions are discretized with velocity grids that are local in time and space, contrary to standard discrete velocity or discrete ordinates methods. The local grids dynamically adapt to time and space variations of the support of the distribution function, by using the conservation laws.

This method is very efficient in case of strong variations of the temperature, for which a standard discrete velocity method requires a very large number of velocities. Moreover, it allows to eliminate the plateau phenomenon in very rarefied regimes.

The extension of this method to 2D problems is in progress and will be presented in a forthcoming work.

However, several aspects of the method should be better understood, in particular, why are there some oscillations if the moment correction step is not used, in the rarefied and free transport regimes, even with high order ENO interpolation? A mathematical analysis of the numerical method could be interesting here.

References

[1] V.V. Aristov. Method of adaptative meshes in velocity space for the intense shock wave problem. *USSR J. Comput. Math. Math. Phys.*, 17(4):261–267, 1977.

[2] C. Baranger, J. Claudel, N. Herouard, and L. Mieussens. Locally refined discrete velocity grids for deterministic rarefied flow simulations. *AIP Conference Proceedings*, 1501(1):389–396, 2012.

[3] G.A. Bird. *Molecular Gas Dynamics and the Direct Simulation of Gas Flows*. Oxford Science Publications, 1994.

[4] A. V. Bobylev and S. Rjasanow. Fast deterministic method of solving the Boltzmann equation for hard spheres. *Eur. J. Mech. B Fluids*, 18(5):869–887, 1999.

[5] A.V. Bobylev, A. Palczewski, and J. Schneider. A Consistency Result for a Discrete-Velocity Model of the Boltzmann Equation. *Siam J. Numer. Anal.*, 34(5):1865–1883, 1997.

[6] C. Buet. A Discrete-Velocity Scheme for the Boltzmann Operator of Rarefied Gas Dynamics. *Transp. Th. Stat. Phys.*, 25(1):33–60, 1996.

[7] Songze Chen, Kun Xu, Cunbiao Lee, and Qingdong Cai. A unified gas kinetic scheme with moving mesh and velocity space adaptation. *Journal of Computational Physics*, 231(20):6643 – 6664, 2012.

[8] J. Claudel, C. Baranger, N. Herouard, and L. Mieussens. Construction of a locally refined discrete velocity grid for deterministic rarefied flow simulations. in preparation.

[9] F. Filbet and T. Rey. A Rescaling Velocity Method for Dissipative Kinetic Equations - Applications to Granular Media. 27 pages, 2012.

[10] U. Fjordholm, S. Mishra, and E. Tadmor. Eno reconstruction and eno interpolation are stable. *Foundations of Computational Mathematics*, 13:139–159, 2013.

[11] J.R.Haack and I.M. Gamba. Conservative deterministic spectral boltzmann solver near the grazing collisions limit. *AIP Conference Proceedings*, 2012.

[12] V.I. Kolobov and R.R. Arslanbekov. Towards adaptive kinetic-fluid simulations of weakly ionized plasmas. *Journal of Computational Physics*, 231(3):839 – 869, 2012.

[13] V.I. Kolobov, R.R. Arslanbekov, V.V. Aristov, A.A. Frolova, and S.A. Zabelok. Unified solver for rarefied and continuum flows with adaptive mesh and algorithm refinement. *Journal of Computational Physics*, 223(2):589 – 608, 2007.

[14] V.I. Kolobov, R.R. Arslanbekov, and A.A. Frolova. Boltzmann solver with adaptive mesh in velocity space. In *27th International Symposium on Rarefied Gas Dynamics*, volume 133 of *AIP Conf. Proc.*, pages 928–933. AIP, 2011.

[15] L. Mieussens. Discrete-velocity models and numerical schemes for the Boltzmann-BGK equation in plane and axisymmetric geometries. *J. Comput. Phys.*, 162:429–466, 2000.

[16] V.A. Panferov and A. G. Heintz. A new consistent discrete-velocity model for the boltzmann equation. *Mathematical Methods in the Applied Sciences*, 25(7):571–593, 2002.

[17] P.Woodward and P.Colella. The numerical simulation of two-dimensional fluid flow with strong shocks. *J. Comput. Phys.*, 54:115–173, 1984.

[18] F. Rogier and J. Schneider. A Direct Method For Solving the Boltzmann Equation. *Transp. Th. Stat. Phys.*, 23(1-3):313–338, 1994.

[19] C.-W. Shu. Essentially non-oscillatory and weighted essentially non-oscillatory schemes for hyperbolic conservation laws. Technical Report 97-65, ICASE, 1997.

[20] S. Takata, Y. Sone, and K. Aoki. Numerical analysis of a uniform flow of a rarefied gas past a sphere on the basis of the boltzmann equation for hard-sphere molecules. *Physics of Fluids A: Fluid Dynamics*, 5(3):716–737, 1993.

[21] V. A. Titarev. Efficient deterministic modelling of three-dimensional rarefied gas flows. *Communications in Computational Physics*, 12(1):162–192, 2012.

[22] K. Xu and J.-C. Huang. A unified gas-kinetic scheme for continuum and rarefied flows. *J. Comput. Phys.*, 229:7747–7764, 2010.

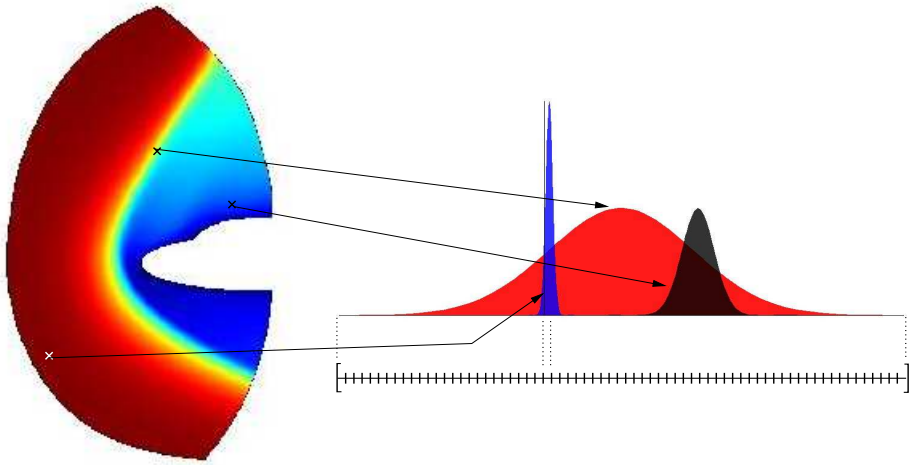

Figure 1: Three distribution functions in different space points of a computational domain for a re-entry problem, and the corresponding global discrete velocity grid $\mathcal{V}$.

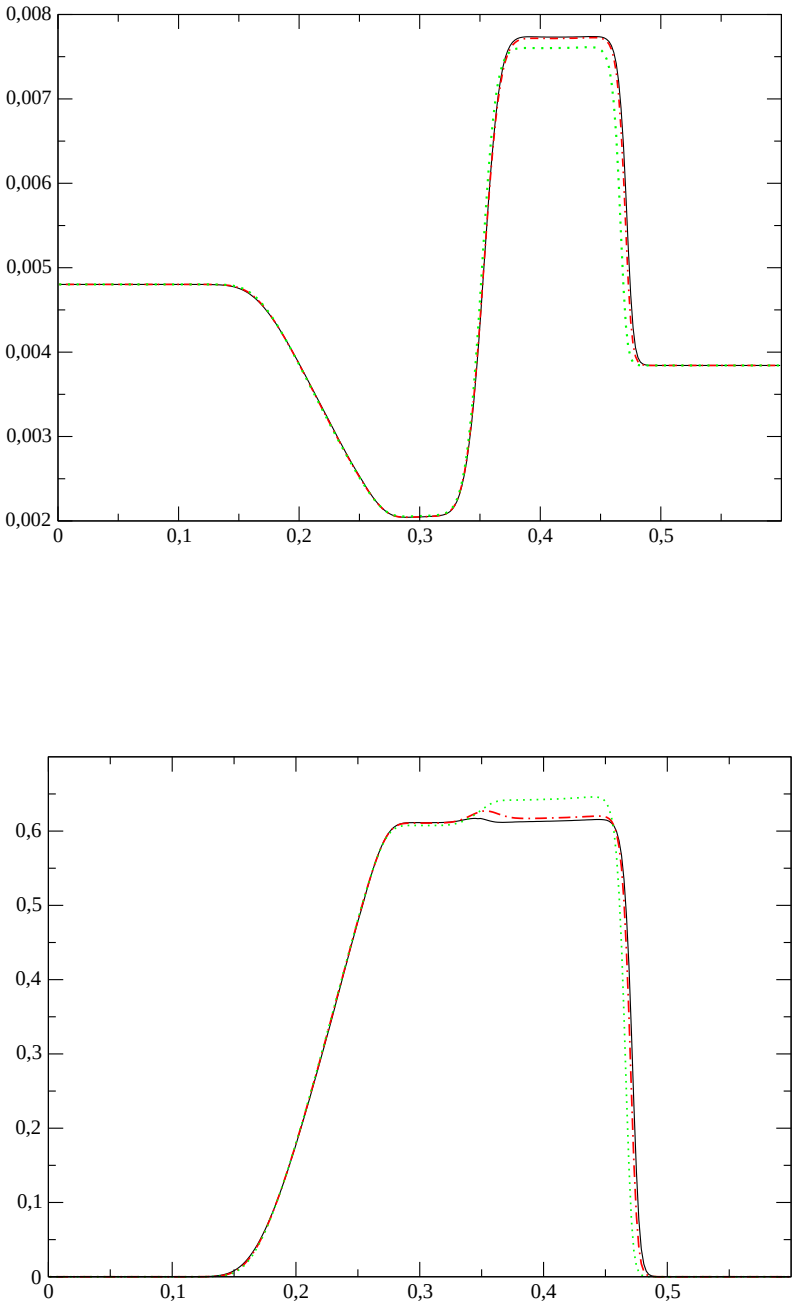

Figure 2: Sod test case, rarefied regime: temperature (top) and velocity (bottom) profiles, at time 7.34 10^{-2}. The solid line is reference solution obtained with the DVM with the enlarged global grid (600 points), the dotted line is the DVM with an incorrect grid (100 points), while the dot-dashed line is the LDV method (30 points).

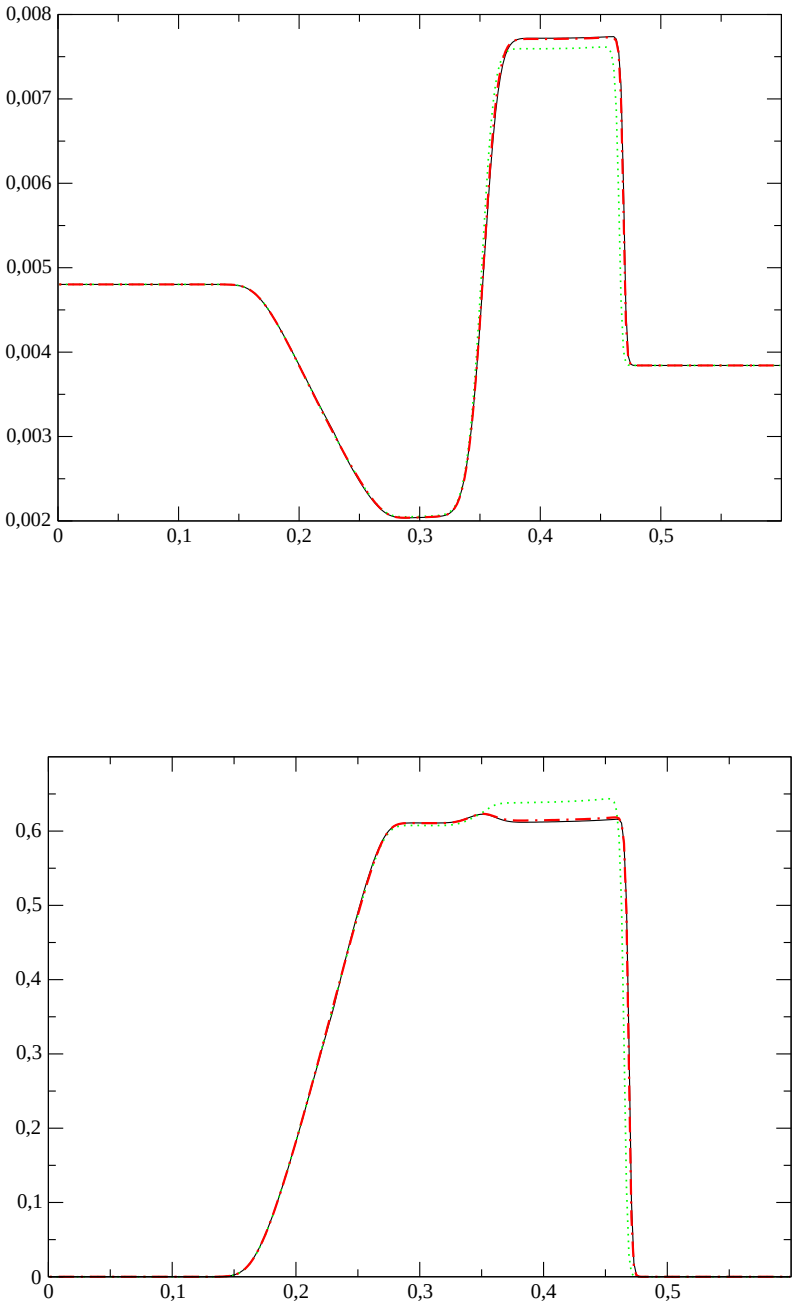

Figure 3: Sod test case, fluid regime: temperature (top) and velocity (bottom) profiles, at time 7.34 10^{-2}. The solid line is reference solution obtained with the DVM with the enlarged global grid (100 points), the dotted line is the DVM with an incorrect grid (100 points), while the dot-dashed line is the LDV method (10 points).

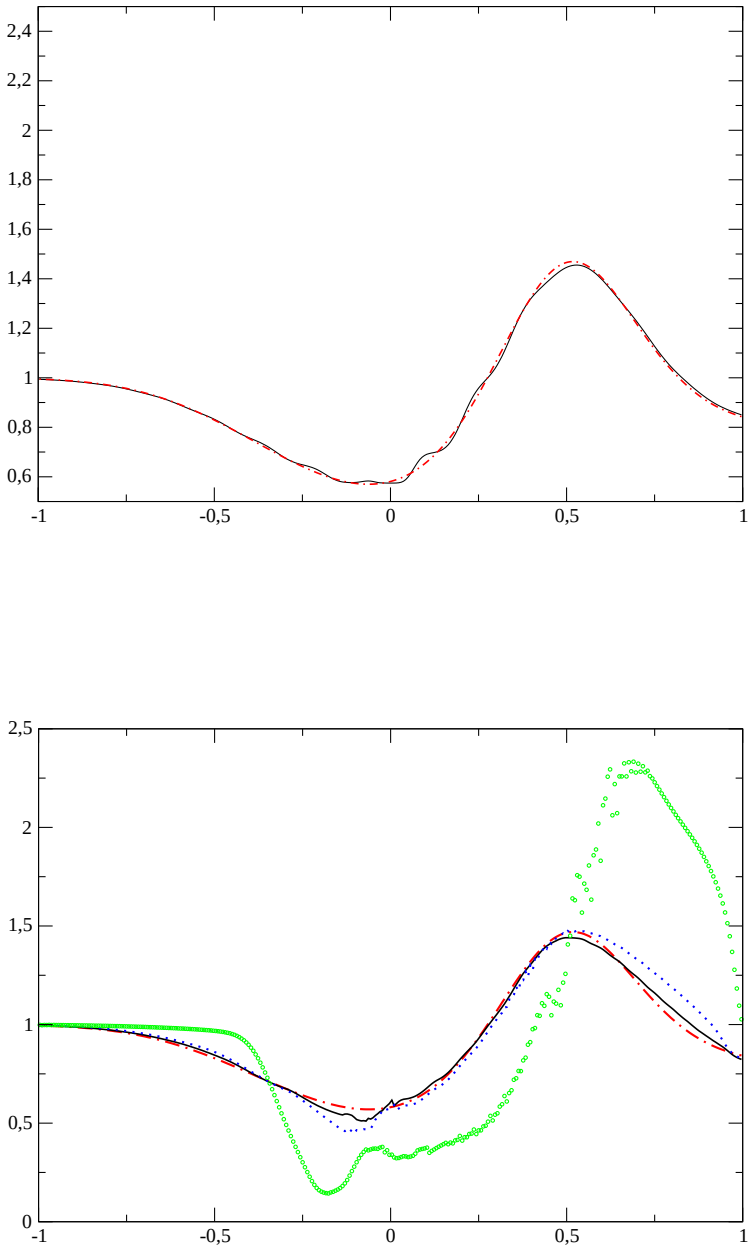

Figure 4: Sod test case, free transport: temperature at time 0.3. Top: comparison between the exact solution (dot-dashed) and with a 30 points DVM (solid). Bottom, comparison between the exact solution (dot-dashed) and several LDVs with 30 points: without ENO ('o'), with 3 points-ENO (dotted), with 4 points-ENO (solid).

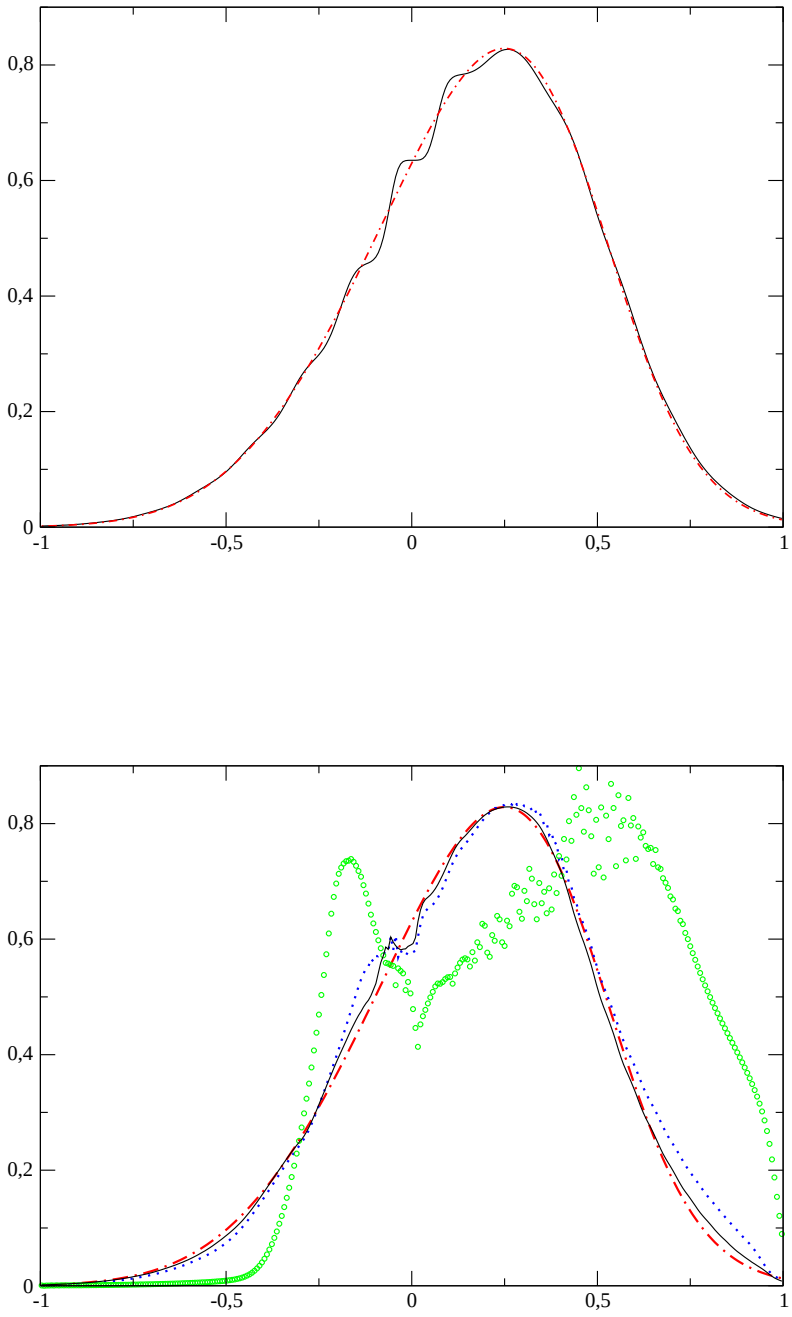

Figure 5: Same as figure 4 for the velocity.

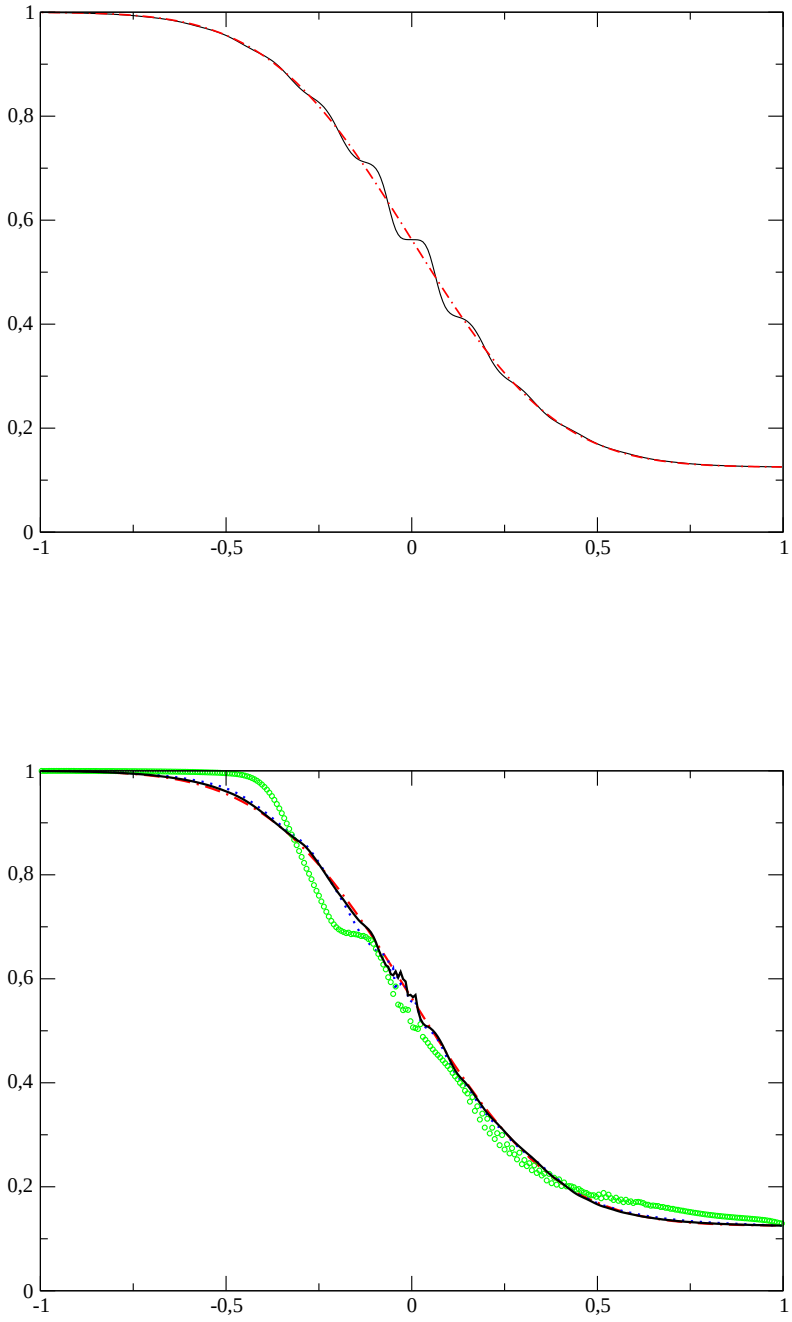

Figure 6: Same as figure 4 for the density.

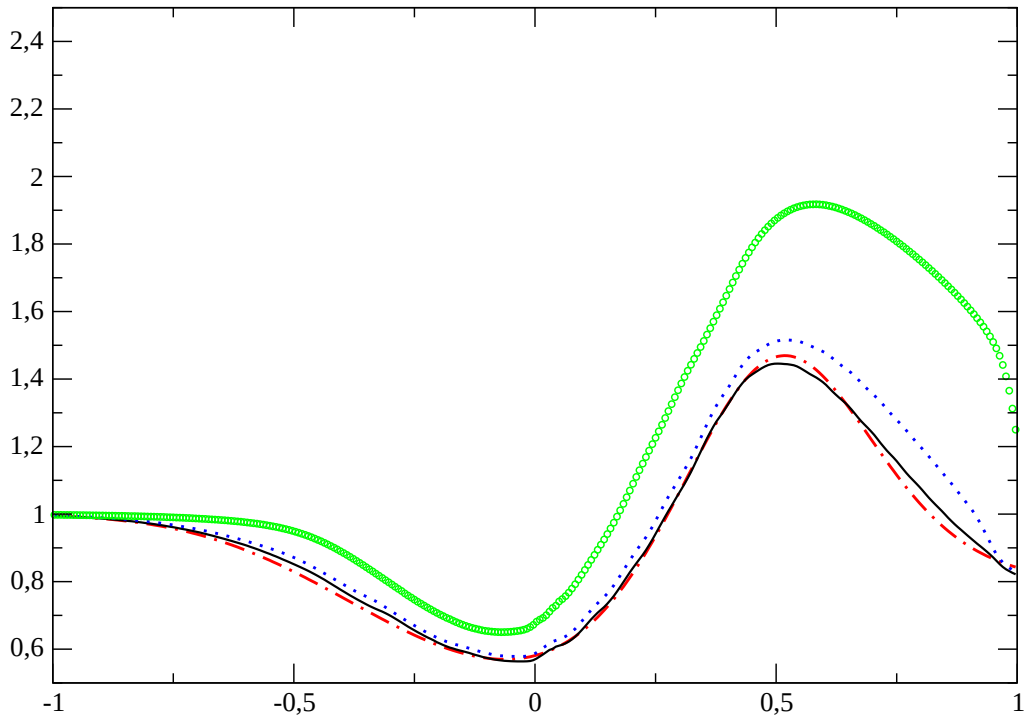

Figure 7: Sod test case, free transport: temperature at time 0.3, comparison between the exact solution (dot-dashed) and several LDVs with 30 points and the moment correction step: without ENO ('o'), with 3 points-ENO (dotted), with 4 points-ENO (solid).

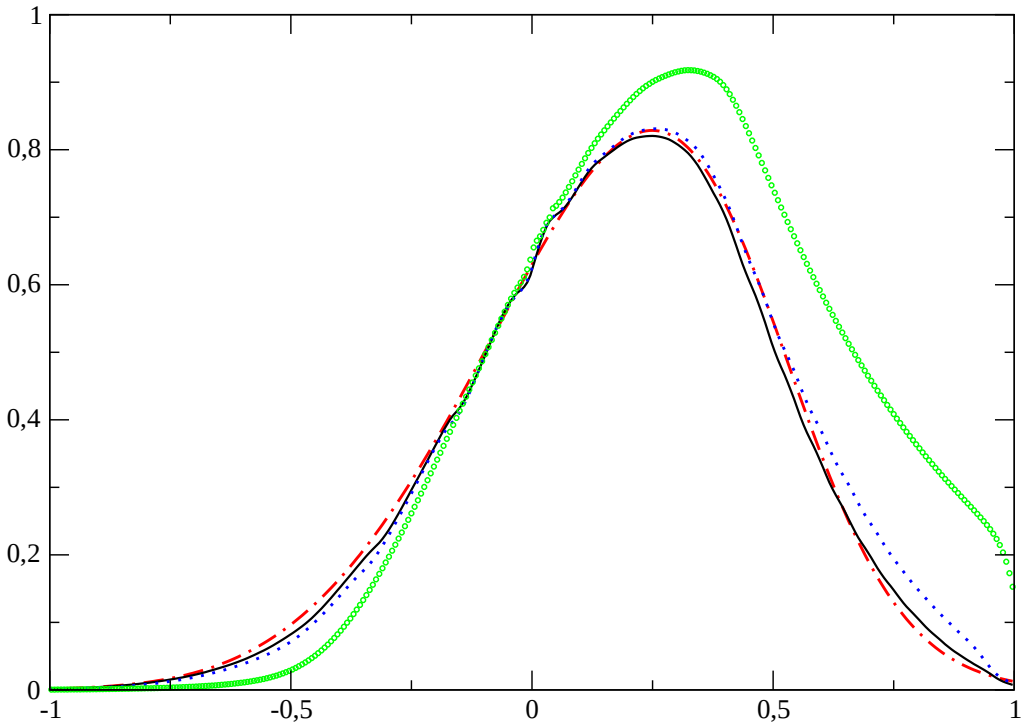

Figure 8: Sod test case, free transport: velocity at time 0.3, comparison between the exact solution (dot-dashed) and several LDVs with 30 points and the moment correction step: without ENO ('o'), with 3 points-ENO (dotted), with 4 points-ENO (solid).

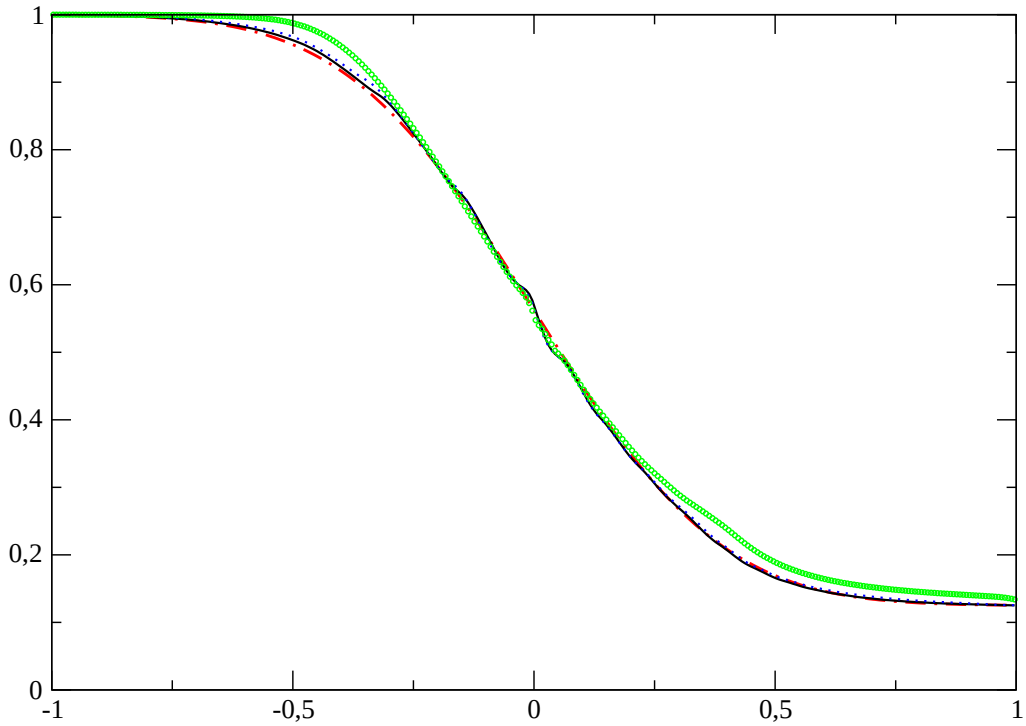

Figure 9: Sod test case, free transport: density at time 0.3, comparison between the exact solution (dot-dashed) and several LDVs with 30 points and the moment correction step: without ENO ('o'), with 3 points-ENO (dotted), with 4 points-ENO (solid).

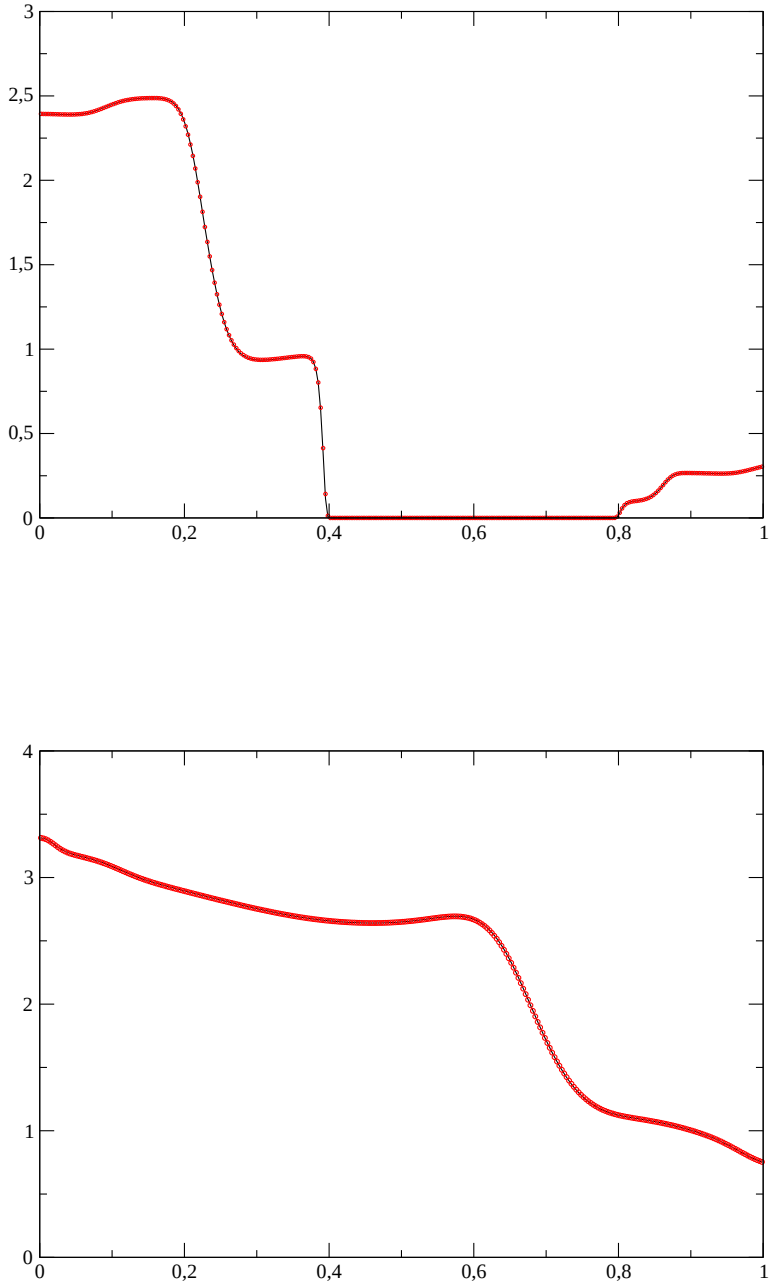

Figure 10: "Two interacting blast waves": Temperature, before the choc at time 0.008 (top) and after the choc at time 0.02 (bottom). The solid line is the solution obtained with the LDV method (30 points), the dotted line is the solution computed with the DVM method (2 551 velocities).

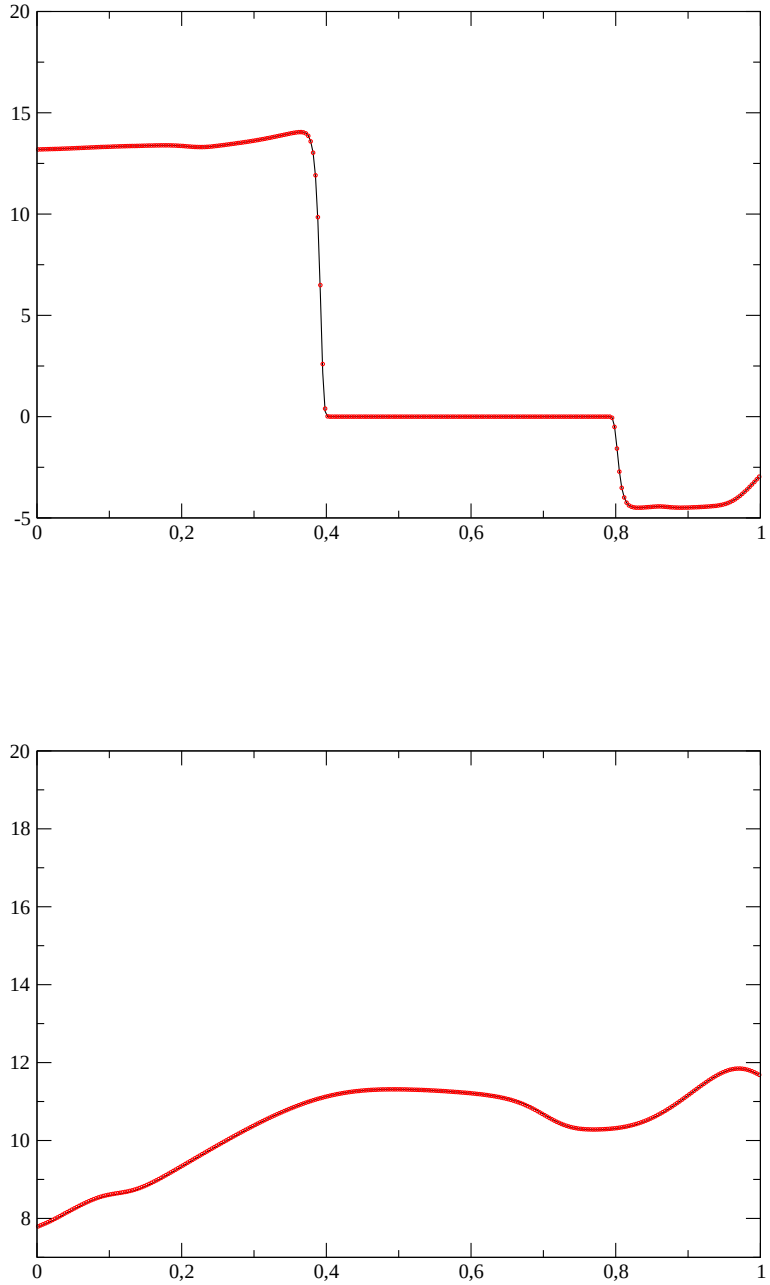

Figure 11: "Two interacting blast waves": velocity (same as figure 10).

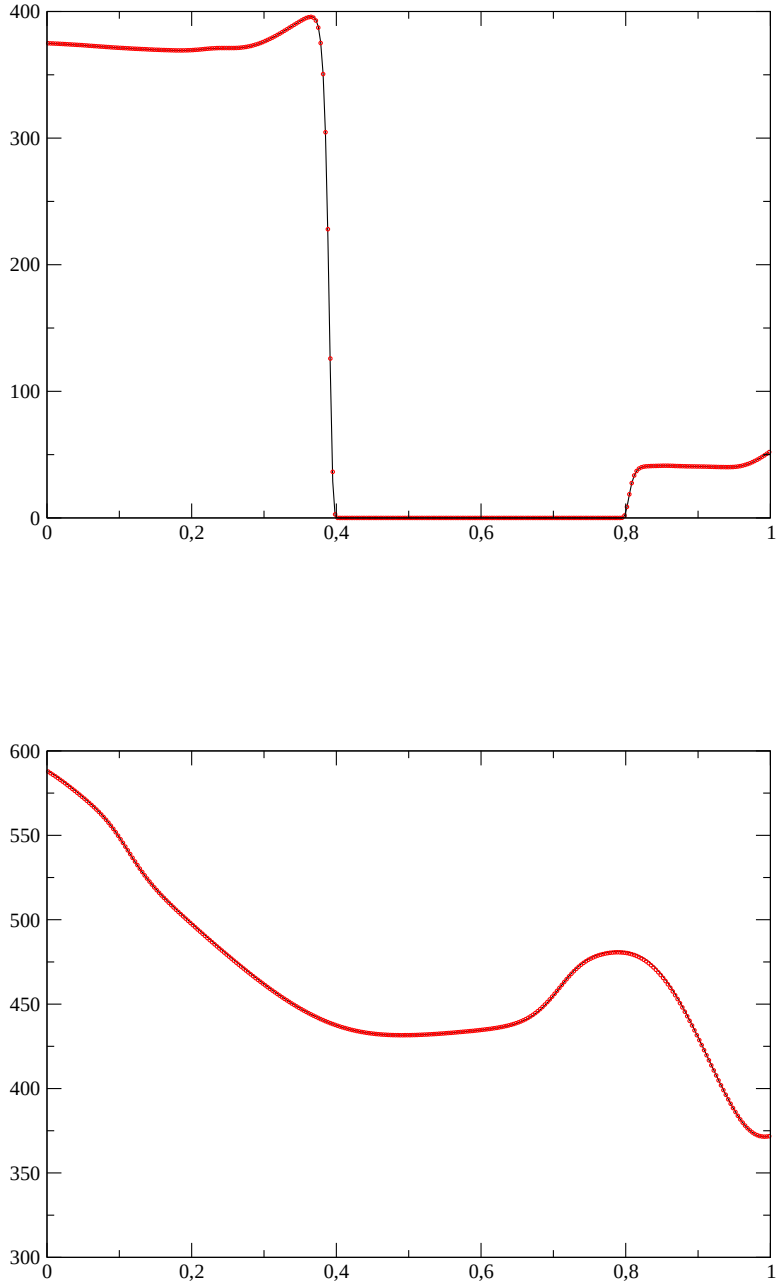

Figure 12: "Two interacting blast waves": pressure (same as figure 10).

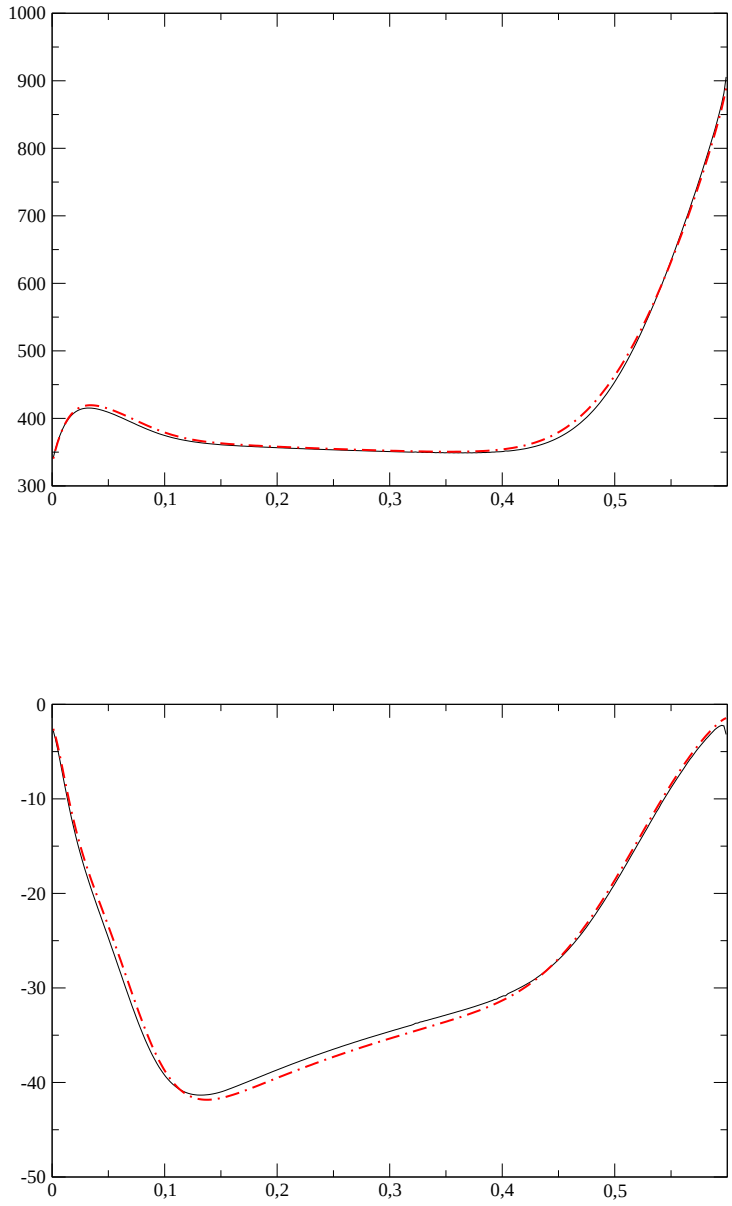

Figure 13: Heat transfer problem, transitional regime: temperature (top) and velocity (bottom) at time $1.3\,10^{-3}$, $Kn = 10^{-2}$. The solid line is the solution given by the LDV method (30 velocities), the dotted line is the DVM method (30 velocities).

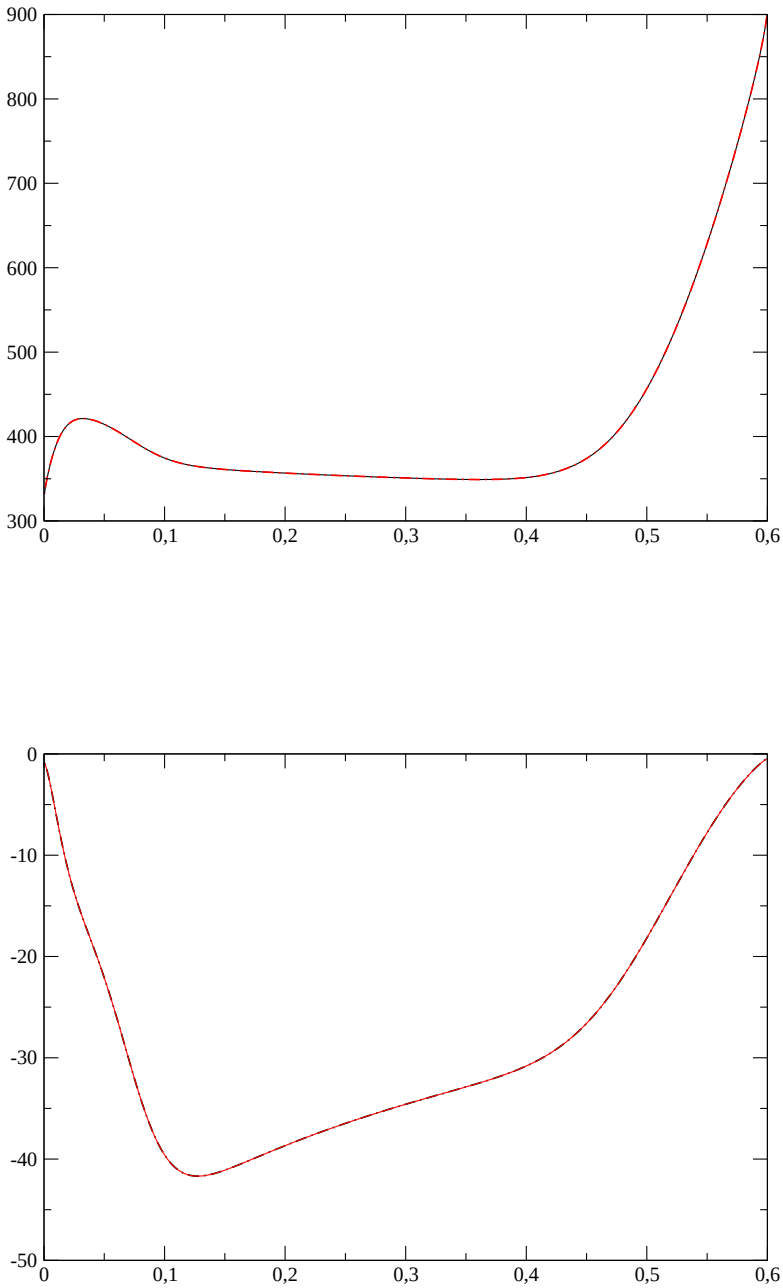

Figure 14: Heat transfer problem, transitional regime (test of the non symmetric local grid): temperature (top) and velocity (bottom) at time $1.3\,10^{-3}$, $Kn = 10^{-2}$. The solid line is the solution given by the LDV method (30 velocities), the dotted line is the DVM method (30 velocities).

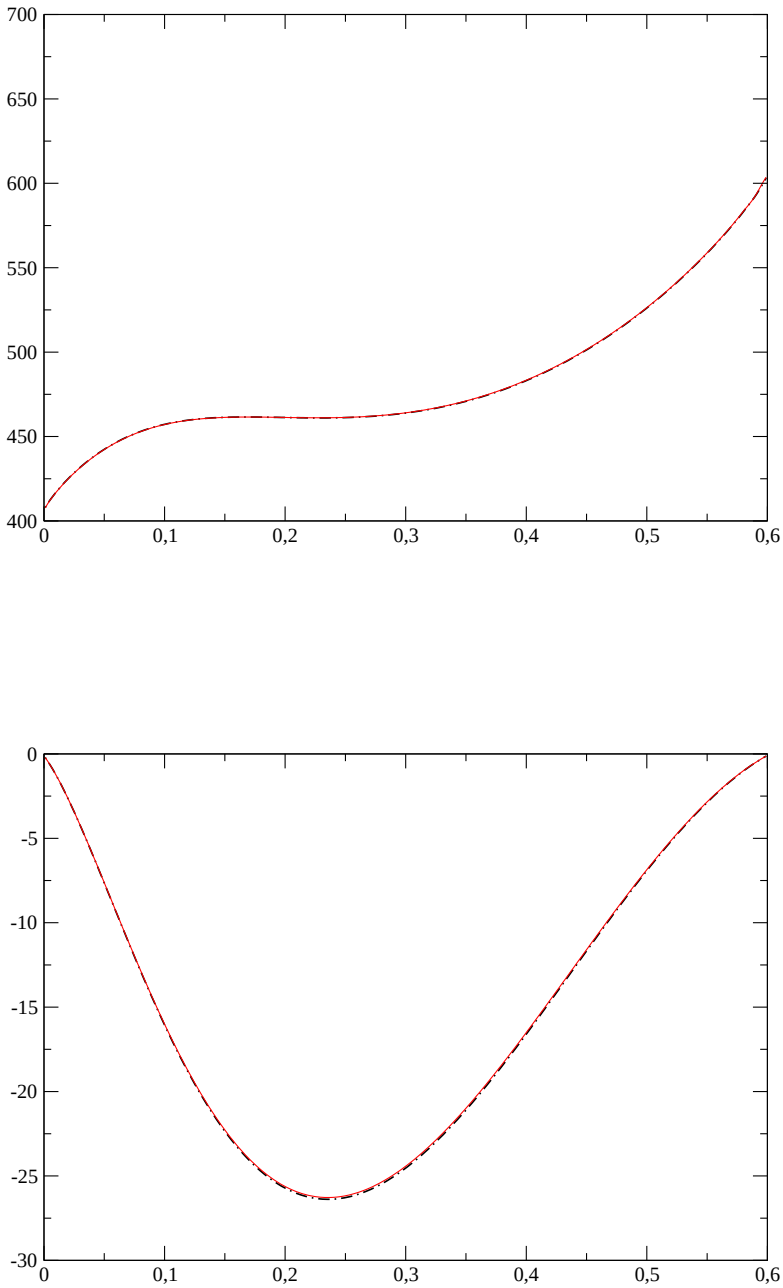

Figure 15: Heat transfer problem, rarefied regime: temperature (top) and velocity (bottom) at time $1.3\,10^{-3}$, $Kn = 1$. The solid line is the solution given by the LDV method (300 velocities, non symmetric local grids), the dotted line is the DVM method (300 velocities).

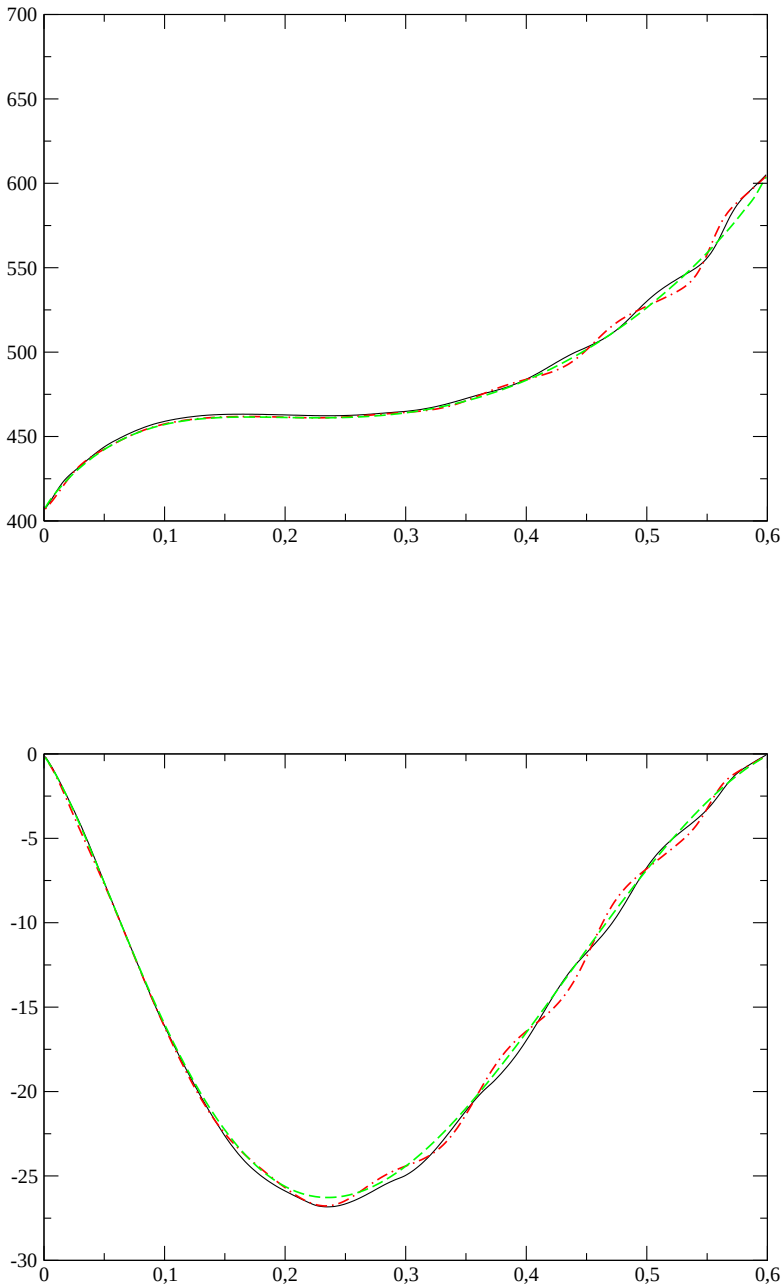

Figure 16: Heat transfer problem, rarefied regime: temperature (top) and velocity (bottom) at time $1.3\,10^{-3}$, $Kn = 1$. The solid line is the solution given by the LDV method (50 velocities, non symmetric local grids), the dotted line is the DVM method (50 velocities), the dashed line is the DVM method with 300 velocities (reference solution).